Article

Proton Displacements Coupled to Primary Electron Transfer in the *Rhodobacter sphaeroides* Reaction Center

Thomas J. Eisenmayer,[†] Jorge A. Lasave,[‡] Adriano Monti,[†] Huub J. M. de Groot,[†] and Francesco Buda*[,†]

[†]Leiden Institute of Chemistry, Leiden University, Einsteinweg 55, P.O. Box 9502, 2300 RA Leiden, The Netherlands
[‡]Instituto de Física Rosario (UNR-CONICET), 27 de Febrero 210 bis, 2000, Rosario, Argentina

S *Supporting Information*

ABSTRACT: Using first-principles molecular dynamics (AIMD) and constrained density functional theory (CDFT) we identify the pathway of primary electron transfer in the *R. Sphaeroides* reaction center from the special pair excited state (P*) to the accessory bacteriochlorophyll (B_A). Previous AIMD simulations on the special pair ($P_L P_M$) predicted a charge-transfer intermediate formation through the excited-state relaxation along a reaction coordinate characterized by the rotation of an axial histidine (HisM202). To account for the full electron transfer we extend the model to include the primary acceptor B_A. In this extended model, the LUMO is primarily localized on the acceptor B_A and extends over an interstitial water (water A) that is known to influence the rate of electron transfer (Potter et al. *Biochemistry* **2005** *280*, 27155−27164). A vibrational analysis of the dynamical trajectories gives a frequency of 30−35 cm^{-1} for a molecular motion involving the hydrogen-bond network around water A, in good agreement with experimental findings (Yakovlev et al. *Biochemistry*, **2003**, *68*, 603−610). In its binding pocket water A can act as a switch by breaking and forming hydrogen bonds. With CDFT we calculate the energy required to the formation of the charge-separated state and find it to decrease along the predicted anisotropic reaction coordinate. Furthermore, we observe an increased coupling between the ground and charge-separated state. Water A adapts its hydrogen-bonding network along this reaction coordinate and weakens the hydrogen bond with HisM202. We also present AIMD simulations on the radical cation (P•+) showing a weakening of the hydrogen bond between HisL168 and the 3¹-acetyl of P_L. This work demonstrates how proton displacements are crucially coupled to the primary electron transfer and characterizes the reaction coordinate of the initial photoproduct formation.
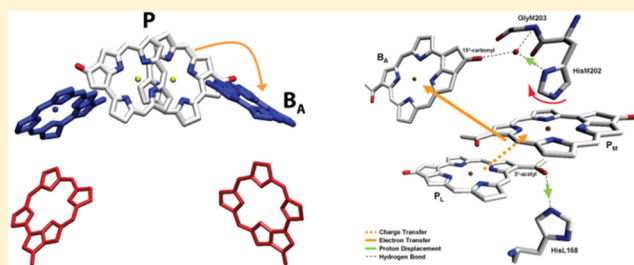
INTRODUCTION

In bacterial photosynthesis, sunlight is absorbed by antenna complexes that transfer the excitation energy to reaction centers where the photoinduced charge separation takes place.[1] The transition state of the primary photochemical reaction in the *Rhodobacter sphaeroides* reaction center (bRC) is not reached through random thermal motion but through specific vibrational coherences that effectively remove the barrier for charge separation.[1,2] This mechanism is of interest for artificial devices aiming for high-yield and barrierless photon-to-charge conversion. The frequencies of these promoting vibrations are well-known from time-resolved spectroscopy,[3−9] yet their structural interpretation is under current debate. Therefore, atomistic simulations are important because they can provide access to structural information not readily available by spectroscopic methods. From the phenomenological study of Novoderezhkin and coworkers based on Redfield theory[2] we know that the formation of the first photoproduct is best described by two vibrational coherences: a fast component of 100−150 cm^{-1} and a slower component of 30−35 cm^{-1}. The time scale of the primary photoinduced processes in bRC is only 3 ps,[10] and it occurs selectively along one of two pseudosymmetric cofactor branches (Figure 1) as:

$$P* \rightarrow (P_L^+ P_M^-) \rightarrow (P_L P_M)^+ B_A^-$$
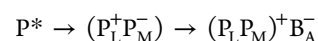
where P* indicates the excited state of the bacteriochlorophyll dimer called the "special pair" (P), ($P_L^+ P_M^-$) is a partial charge-transfer (CT) intermediate,[11,12] and B_A is the accessory bacteriohlorophyll acting as primary acceptor. Subsequent electron transfer (ET) to form the secondary photoproduct along the A-branch, a reduced bacteriopheophytin (H_A^-), is very fast (1 ps). In this context, it is our aim to accurately characterize the reaction coordinate of the primary photo-induced charge separation from first principles. In previous work on the special pair, excited-state dynamics combined with a frequency analysis showed that a ~100 cm^{-1} vibrational mode is coupled to the electronic excitation, leading to a CT intermediate ($P_L^+ P_M^-$).[13] Structurally, this ~100 cm^{-1} mode involves a collective motion of P with most amplitude on P_M and the rotation of HisM202 as the characteristic coordinate. This is predicted to be the first/fast vibrational component that
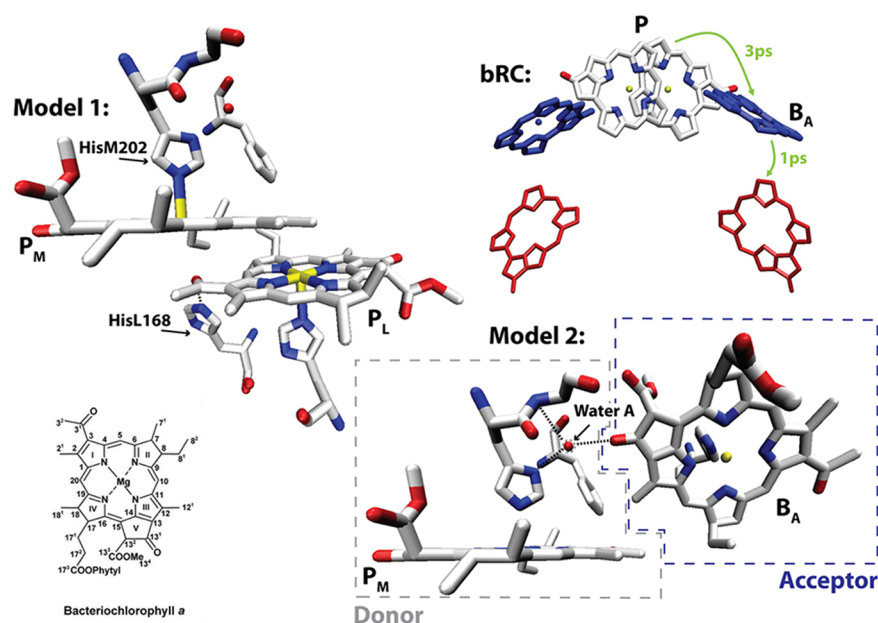
Figure 1. bRC: Two-fold symmetric reaction center of *Rhodobacter sphaeroides* extracted from the latest 2.55 Å resolution X-ray structure (PDB entry 1M3X). The direction of electron transfer and corresponding time scales are denoted in green. **Model 1**: Including the special pair (P), axial histidines (HisL173 and HisM202), water A and B, and the diagonal symmetry-breaking residues PheM197 and HisL168. **Model 2**: Water A, the donor P_M, the primary acceptor B_A, the axial histidines (HisM202 and HisL153), and GlyM203. (See the SI for an explanation of excluding P_L.) **Inset**: Bacteriochlorophyll numbering.

modulates the transient absorption signal.[2] HisM202 is hydrogen bonded to an interstitial water (water A), which is held in place by a hydrogen-bond network connecting P_M and B_A. The loss of water A through site-directed mutation is accompanied by a slowing of the rate of ET by a factor of 8.[14] The second/slower vibrational component coupled to full charge separation is thus attributed to the motion of water A with a frequency of ~30−35 cm^{-1}.[15]

The breaking of symmetry between cofactor chains is intimately related with the forward CT reactions. The concerted motion of protein and chromophore coupled to forward ET may constitute the prime symmetry-breaking principle. Although the special pair itself is already surrounded by the protein environment in a quasi-symmetric fashion (see Figure 1), on the L-side, HisL168 forms a hydrogen bond with the 3^1-acetyl of P_L, whereas on the M-side PheM197 does not. It is therefore plausible that even before excitation of P the ground-state electron density is asymmetrically distributed.[16,17] The vibrational mode corresponding to the hydrogen bond between P_L and HisL168 has been calculated to have a frequency of ~50 cm^{-1}, and it is found to affect the stability of the cation (P$^{•+}$).[13,18]

In this article we employ atomistic simulations and single-point calculations to address (i) the role of the interstitial water A and (ii) the coupling of the ET process to configurational changes following the excitation and (iii) upon oxidation of P. We perform first-principles molecular dynamics (AIMD)[19,20] in the ground, excited, and oxidized state of P to find the structural motifs accompanying vibrational coherence in bRC and constrained density functional theory (CDFT)[21] to sample the ET energy as a function of the suggested reaction coordinate and to calculate the electronic coupling parameter (H_{AB}) before and after rotation of HisM202. We consider two models fully described quantum mechanically within DFT: Model **1** including the special pair and surrounding residues

and Model **2** involving P_M, the primary acceptor B_A and the residues surrounding water A (see Figure 1).

From the special pair model (Model **1**) we find that the rotation of HisM202 in the excited state is reversible upon oxidation. The important degree of freedom that is found to change upon oxidation is the hydrogen bond between the 3^1-acetyl of P_L and HisL168, involving a proton displacement that destabilizes the HOMO on P_L.[13] From the donor−acceptor model (Model **2**) water A is found to be stable throughout the dynamics in its hydrogen-bonding network, albeit forming and breaking hydrogen bonds. Noticeably, water A can act as a switch using its two protons to alternate hydrogen bonds with the 13^1-carbonyl of B_A. The hydrogen bond with HisM202 is weakened and strengthened during the dynamics but overall stable. Fourier transforms of different parameters involved in the hydrogen-bond network give a frequency of 30−35 cm^{-1}, in nice agreement with experiment for the switching motion between the two protons of water A and the carbonyl of B_A. CDFT calculations show that a displacement along the predicted first reaction coordinate of charge separation decreases the ET energy, increases the donor−acceptor coupling and involves a proton displacement. Together, these results add to an atomistic understanding of the coherent and highly efficient primary charge separation in bRC.

■ MODEL AND METHODS

We extract the special pair (Model **1**) and the donor−acceptor model (Model **2**) from the latest X-ray crystallographic data of wild-type *Rhodobacter sphaeroides* at 2.55 Å resolution.[22] The special pair Model **1** includes the two bacteriochlorophylls P_M and P_L, the five closest amino acids (GlyM203, PheM197, HisM202, HisL173, HisL168), and two interstitial waters (Figure 1). The donor−acceptor Model **2** includes P_M and its axially coordinated HisM202, taken as the donor of charge. B_A and its axially coordinated histidine HisL153 are taken as the

charge acceptor (Figure 1). We also include PheM197 and GlyM203 to keep the whole protein pocket environment for the water A. For the entire system—Model **1** combined with Model **2**—we find that the HOMO and LUMO are localized on P_M and B_A, respectively, consistently with Model **2** (see the SI). Moreover, the HOMO−LUMO gap is not significantly altered (∼0.04 eV) and this therefore justifies the exclusion of P_L from Model **2** to keep the system size minimal. The mechanical constraints induced by the protein environment are ensured by fixing the tails of the histidines, the phenylene, and the glycine. Because of their length the phytyl side chains are sterically hindered within the protein and are known not to affect the electronic structure of the bacteriochlorophylls.[17] Therefore they are reduced to a methyl group that is fixed. The full set of initial atomic coordinates included in the models is given in the SI.

The AIMD simulations have been performed using the Car−Parrinello method as implemented in the CPMD code[23] with a time step of 0.1 fs. A Nosé thermostat is used in all simulations to keep the temperature around an average of 300 K. The time scales of the simulation runs for Model **1** are chosen to be ∼1 ps for ground, excited, and radical cation states. For Model **2** a ground-state simulation is performed for ∼2 ps. It should be stressed that this simulation is not aimed at the explicit description of the real-time (∼3 ps) ET from P* to B_A that would require a time evolution of the excited electronic state. The main goal of this AIMD simulation is to investigate the stability of the interstitial water and the thermal fluctuations in the hydrogen-bonding network established between the donor and acceptor. Both models are stable along the dynamics with a root-mean-square displacement (RMSD) that fluctuates around an average value of 0.8 Å for Model **2**, slightly larger than the RMSD of Model **1** (0.6 Å).

The BLYP functional[24,25] is used for the exchange-correlation energy, which is known to yield hydrogen bonds that are in good agreement with experiment. The Kohn−Sham orbitals are expanded in a plane-wave basis set with an energy cutoff of 70 Ry. We employ dispersion-corrected atom-centered (DCACP) pseudopotentials.[26,27] To study the frequency domain, we perform Fourier transforms of the velocity autocorrelation function of the AIMD trajectory. We can in this way obtain specific characteristic frequencies of individual structural parameters (i.e., bond distances, bond angles).

The recently developed computational method of CDFT is used to verify the predicted reaction coordinate of primary charge separation. This method was specifically developed by Wu and van Voorhis[21] to address long-range CT states. It has been shown that CDFT can accurately describe the excitation energy and its dependence on the donor−acceptor distance.[28] The CDFT calculations are performed with the same functional, basis set, and pseudopotentials used for the AIMD simulations. In the CDFT method applied to bRC, the charge-localized states (or diabatic states) A and B are obtained from two DFT calculations. The first represents the initial state where no ET between donor and acceptor has occurred yet (state A), while the second (state B) describes the charge-separated state obtained by constraining a positive charge on the donor and a negative charge on the acceptor. The resulting ground-state density $\rho(r)$ on each diabatic state will satisfy the constraint

$$\int w(r)\rho(r)\ \mathrm{d}r = N_c$$

where $w(r)$ is the operator that defines the electronic population and the integral runs over the entire volume of the system. N_c is the value of the constraint defined as the charge difference between the net charge on the donor and acceptor group: $N_c = (N_{don} − N_{acc})$. Therefore, we choose $N_c = 0$ for state A and $N_c = 2$ for state B. For the population operator we use the Hirshfeld partitioning scheme[29] as implemented in the CPMD code.[30]

■ RESULTS

AIMD Simulations. Previous AIMD simulations on the special pair (Model **1**) ground and excited state found two important degrees of freedom coupled to electronic structure rearrangements of P: (1) the rotation of HisM202 with respect to the Mg−N_τ coordination axis and (2) the hydrogen bond between P_L and HisL168.[13] Here we extend these simulations to analyze the oxidized radical cation state. The first degree of freedom and characteristic coordinate of the vibrational mode coupled to the formation of the CT intermediate involves the rotation of the axial histidine M202. From Figure 2, which
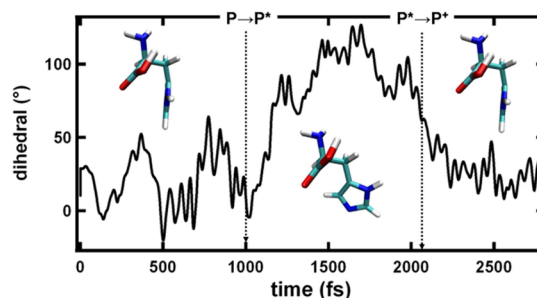

Figure 2. AIMD simulations of Model **1** showing the time evolution of HisM202 dihedral angle with respect to the Mg−N_τ coordination axis along the ground state (0 to 1.0 ps), excited state (1.0 to 2.1 ps), and oxidized state (2.1 to 2.8 ps) trajectories.

shows the compiled trajectories for ground state, excited state, and radical cation, it can be seen that HisM202 rotates upon excitation to an average dihedral angle of 80° with respect to the Mg−N_τ coordination axis. Upon oxidation this conformational rearrangement is reversed and the dihedral angle rotates back to the ground-state values. Inversely, the second important degree of freedom involving the hydrogen bond between the 3^1-acetyl of P_L and HisL168 (see Figure 1) shows no significant changes going from ground to excited state. However, upon oxidation the oscillations become larger and the hydrogen bond is on average weakened (Figure 3).

On the donor−acceptor model (Model **2**) a room-temperature AIMD simulation is performed extending over 2 ps. DFT single-point calculations performed at several snapshots along the trajectory show consistently that the HOMO is localized on P_M and the LUMO is localized on B_A. The LUMO electron density extends over the interstitial water A, whereas the HOMO shows no electron density in this region, although it does extend over the axial histidine M202. To understand the structural cause of HOMO−LUMO localization we investigated the planarity of both chromophores taking into account the C_3−C_7−C_{12}−C_{17} dihedral angle (see inset, Figure 1). P_M is found to be the more distorted chromophore, whereas B_A is almost perfectly planar. Another factor influencing the HOMO−LUMO localization is the orientation of the axial histidines relative to the Mg−N_τ axis. For P_M the dihedral angle
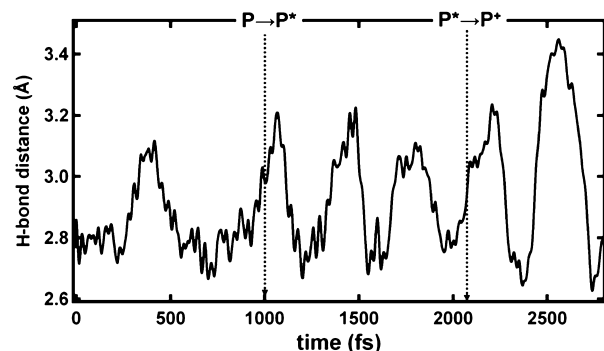
Figure 3. N···O hydrogen-bond distance between HisL168 and the 3^1-acetyl of P_L for ground state (0 to 1.0 ps), excited state (1.0 to 2.1 ps), and radical cation (2.1 to 2.8 ps) AIMD trajectories. Upon excitation no changes in the amplitude of the fluctuations are observed, whereas in the radical cation state the hydrogen bond is weakened, representing a proton displacement.

of the axially coordinated histidine, averaged over the dynamics, is 21°, whereas for B_A this angle is −108°. The position of water A in its hydrogen-bond network is stable throughout the dynamics. The average position of water A is halfway between the HisM202-nitrogen and the 13^1-keto-carbonyl. Figure 4
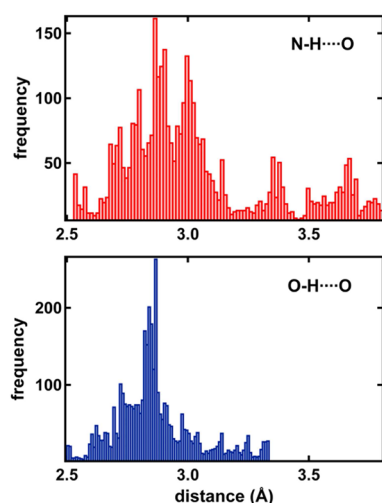

Figure 4. Distribution of distances centered around the interstitial water A oxygen atom sampled during the AIMD simulations of Model **2** in the ground state. Top graph (red) distribution of N−H···O distances representing the hydrogen bond with His M202. Bottom graph (blue) distribution of O−H···O distances representing the hydrogen bond with the keto carbonyl of B_A.

shows the distribution of N−H···O and O−H···O distances. The most frequently occurring separation is ∼2.8 Å for both degrees of freedom. The N−H···O distances additionally have a tail at larger separations with peaks at 3.4 and 3.7 Å.

Dynamically, both protons of water A form and break hydrogen bonds with the keto carbonyl of B_A in a "switching" motion (Figure 5a,b). A Fourier analysis of this motion, in terms of hydrogen-bond angles and distances, gives a frequency of 30−35 cm^{-1} for the breaking and forming of the keto carbonyl hydrogen bonds (Figure 5c). The weakest hydrogen bond of water A is with Gly M203, which is rarely formed during the 2 ps ground-state trajectory.

Constrained DFT. To explore the reaction coordinate of excited-state relaxation and ET we performed CDFT
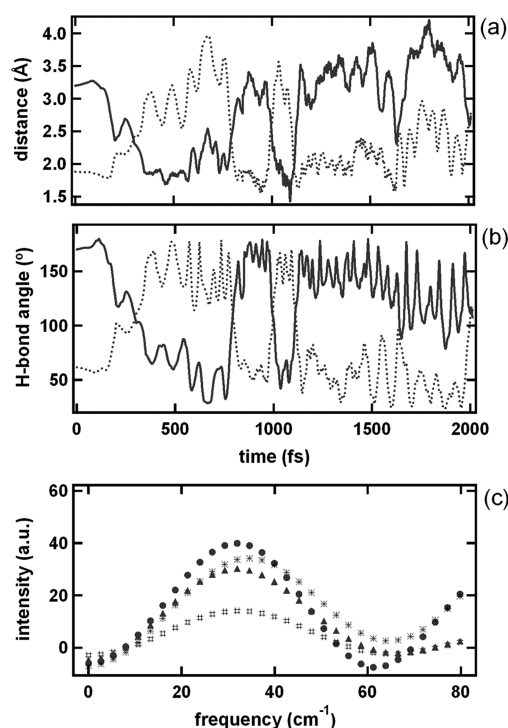
Figure 5. Hydrogen bond H···O distance (a) and O−H···O angle (b) along the dynamical trajectory. The full and dotted line show the two protons of water A that break and form hydrogen bonds in a "switching" motion with the keto 13^1 carbonyl group of B_A. The bottom graph (c) shows the Fourier transform of this molecular motion between water A and the keto carbonyl group of B_A with a first peak at 30−35 cm^{-1} in agreement with the experimental result of Yakovlev et al.[15]

calculations constraining a positive charge on the donor (P_M) and a negative charge on the acceptor (B_A). Following the HOMO−LUMO analysis, we include the axial histidine HisM202 in the donor and the axial histidine HisL153 in the acceptor. Energies are calculated as a function of the dihedral angle corresponding to the HisM202 rotation (see Figure 2). For each value of the dihedral angle we optimize the other degrees of freedom including the position of water A. The energy difference between the two diabatic states decreases along the suggested reaction coordinate, as shown in Figure 6. In this plot we subtract the photon energy corresponding to the P absorption maximum because we are looking at the P*→ $P^+B_A^-$ process. At the ground-state geometry corresponding to a value of the dihedral angle around 20° we estimate an ET energy of ∼0.6 eV. For this geometry we expect a positive value (larger than the photon energy of ∼1.4 eV) because the charge-separated state ($P^+B_A^-$) is far from the minimum of the corresponding diabatic potential surface. By increasing the value of the dihedral angle the ET energy decreases to 0.4 eV. At the intersection between the two diabatic curves this value should change sign to get a negative driving force (ΔG), which is experimentally estimated to be about −0.06 eV.[31] The positive value of 0.4 eV is partially due to the fact that we have not fully equilibrated the geometry in the CT state; moreover, it can be related to an overestimation of the ET energy by the BLYP functional. Further calculations including entropic effects and different functionals will be needed to explore this issue.

While the ET energy decreases, the electronic coupling between the charge-neutral and charge-separated states
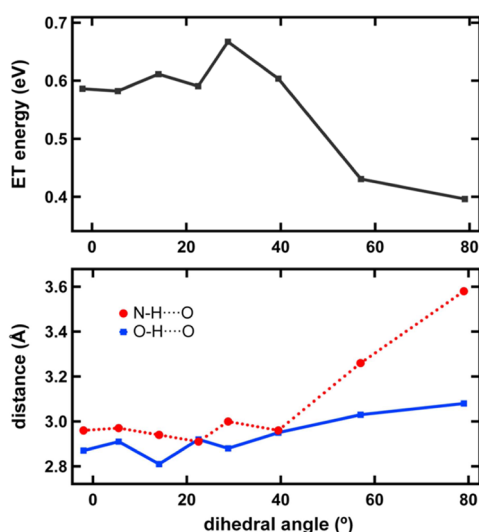
Figure 6. Top: Electron transfer (ET) energy dependence on the dihedral angle of HisM202 with respect to the Mg−N$_\tau$ coordination axis. Bottom: N−H···O (circles) and O−H···O (squares) hydrogen-bond distances as a function of the same dihedral angle.

Figure 7. Scheme of charge-transfer intermediate formation (orange dotted line), HisM202 rotation (red arrow), the proton displacement coupled to this motion involving water A (green arrow), and the proton displacement involving HisL168 and the 3^1-acetyl of P$_L$ (green arrow) upon oxidation (orange arrow).

increases by ∼35% from ∼0.70 to ∼0.95 eV going from a dihedral angle of 14° to 80°. It is beyond the scope of this work to calculate the free energy change (ΔG) and the reorganization energy (λ) that are the parameters needed for estimating the ET rate within a semiclassical Marcus theory.[32] It is also questionable whether Marcus theory could be appropriate for describing such a fast ET process (∼3 ps). If we consider the estimated values for ΔG and λ reported in the literature (see, for example, refs 33 and 34 and references therein) and use the computed value for the coupling parameter H$_{AB}$, then we obtain a rate that is unphysically high. Clearly the values of the coupling parameter H$_{AB}$ obtained with the BLYP functional appear to be severely overestimated. It has been already noticed in the literature that BLYP has the tendency to delocalize the excess electron even under the presence of the constraint potential, thus leading to an overlap of the two diabatic states that is too large.[30] Possibly, the use of hybrid functionals, which is computationally very expensive for the relatively large systems reported here, would give a better estimate of the electronic coupling. For comparison the couplings for heme-to-heme ET have been previously estimated with B3LYP to be on the order of 10 meV at heme separation distances similar to the donor−acceptor distance in this model.[35] Moreover, the coupling parameter may be affected by thermal fluctuations in the protein environment, and ideally one should take an average from a statistically relevant set of configurations. Nonetheless, these results show that even a small proton displacement can have a large effect on the electronic coupling and vertical ET energy.

We find that the rotation of HisM202 displaces water A in its hydrogen-bond pocket toward the carbonyl of B$_A$ and GlyM203 (Figure 7). After ET the N−H···O distance increases to 3.6 Å, representing a considerable weakening of the hydrogen bond between the water and HisM202 (Figure 6). Interestingly, it is apparent that already in the ground state this conformation of the hydrogen-bond network is occasionally sampled (see Figure 4). Thus, our results show no direct evidence of full proton coupled electron transfer (PCET) but clearly indicate a proton displacement coupled to the reaction coordinate.
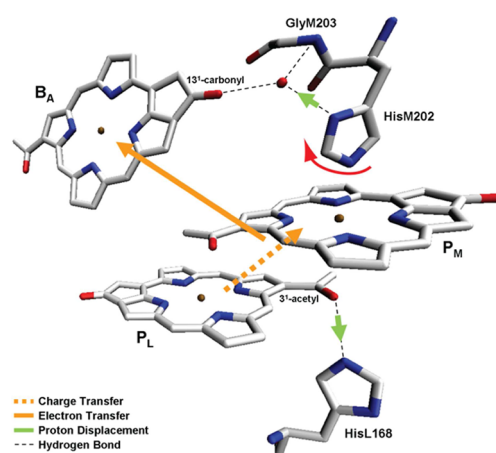
DISCUSSION AND CONCLUSIONS

The variation of the orbital energies in response to specific low-frequency vibrational coordinates gives rise to a time-oscillatory alternation of quantum delocalization of electrons and confinement with partial charge transfer already in the ground state on a subpicosecond time scale.[13] Excitation of the system shifts the balance toward charge transfer along a spatially anisotropic reaction pathway, and the state develops in a coherent manner along another normal coordinate involving both conformational rearrangement and proton displacements. The combined development of the reaction along more than one reaction coordinate allows for a change in chemical topology that is essentially barrierless.[2]

Here we elucidate the conformational rearrangements that couple to full ET to the primary acceptor B$_A$. The coordinate of the excited-state relaxation involves the rotation of HisM202, which is found to be reversible upon oxidation. This rotation displaces the protons of water A toward GlyM203 and the 13^1-carbonyl of B$_A$ in a collinear fashion with respect to the direction of ET (Figure 7). The proton displacement is found to have a frequency of 30−35 cm^{-1} in good agreement with experiment and thus gives a structural interpretation to the second coordinate of charge separation suggested in the phenomenological study by Novoderezhkin and coworkers.[2] In contrast with Ivashin and Larsson, who propose a double proton-transfer mechanism within the hydrogen-bond network surrounding water A,[36] we observe only a proton displacement following ET (Figures 6 and 7). In the ground state, this conformation is already occasionally sampled (Figure 4), although the average distance of water A from HisM202 is 2.9 Å. In the charge-separated state we find a new equilibrium value of 3.6 Å at the same approximate values where the ground-state histogram exhibits a long tail (Figure 4).

The second proton displacement found to couple to oxidation of P involves the weakening of the hydrogen bond between HisL168 and the 3^1-acetyl of P$_L$, representing an orthogonal proton displacement with respect to the direction of ET (Figure 7). The weakening of this interaction destabilizes the HOMO of P$_L$,[13] the site on which most of the positive charge is localized in P$^{•+}$,[37] and therefore reduces the driving force for charge recombination. Experimental evidence for such

a mechanism is possibly given by Deshmukh and coworkers,[38] who find a light-induced hypsochromic shift in *Rhodobacter capsulatus* and suggest this to be caused by the 3^1-acetyl group.

In conclusion, the reaction coordinate of initial charge separation in the *Rhodobacter sphaeroides* reaction center is a multidimensional landscape. First, upon excitation a reversible conformational rearrangement stabilizes the charge transfer from P_L to P_M, mostly involving the rotation of HisM202 with a characteristic frequency of ~ 100 cm^{-1}. Second, through this rotation, which we have shown to increase the coupling between the donor P and the primary acceptor B_A, a proton is displaced in the hydrogen network surrounding water A with a frequency of $30-35$ cm^{-1}. Finally, on a longer time scale, another proton is displaced from the 3^1-acetyl of P_L toward HisL168, which destabilizes the cation $P^{\bullet+}$ and so reduces the driving force for charge recombination. Together these rearrangements present a structural framework for understanding the highly efficient and coherent CT process from the special pair excited state to the primary charge-separated state. Although we believe that this picture is qualitatively correct, there are several methodological issues that need to be addressed to quantitatively describe the full ET process, which remains a computationally challenging problem.

■ ASSOCIATED CONTENT

Ⓢ Supporting Information
HOMO and LUMO orbitals computed for Model **2** and for an extended model including also P_L bacteriochlorophyll. Cartesian coordinates of Models **1** and **2**. This material is available free of charge via the Internet at http://pubs.acs.org.

■ AUTHOR INFORMATION

Corresponding Author
*E-mail: f.buda@chem.leidenuniv.nl. Fax: +31 (0)71 5274603. Tel: +31 (0)71 5275723.

Notes
The authors declare no competing financial interest.

■ ACKNOWLEDGMENTS

■ REFERENCES

(1) Deisenhofer, J.; Epp, O.; Miki, K.; Huber, R.; Michel, H. Structure of the Protein Subunits in the Photosynthetic Reaction Centre of Rhodopseudomonas Viridis at 3Å Resolution. *Nature* **1985**, *318*, 618−624.

(2) Novoderezhkin, V.; Yakovlev, A.; van Grondelle, R.; Shuvalov, V. Coherent Nuclear and Electronic Dynamics in Primary Charge Separation in Photosynthetic Reaction Centers: A Redfield Theory Approach. *J. Phys. Chem. B* **2004**, *108*, 7445−7457.

(3) Vos, M. H.; Jones, M. R.; Hunter, C. N.; Breton, J.; Martin, J. L. Coherent Nuclear Dynamics at Room Temperature in Bacterial Reaction Centers. *Proc. Natl. Acad. Sci. U.S.A.* **1994**, *91*, 12701−12705.

(4) Vos, M. H.; Jones, M. R.; Martin, J. L. Vibrational Coherence in Bacterial Reaction Centers: Spectroscopic Characterisation of Motions Active during Primary Electron Transfer. *Chem. Phys.* **1998**, *233*, 179−190.

(5) Rischel, C.; Spiedel, D.; Ridge, J. P.; Jones, M. R.; Breton, J.; Lambry, J. C.; Martin, J. L. Low Frequency Vibrational Modes in Proteins: Changes Induced by Point-Mutations in the Protein-Cofactor Matrix of Bacterial Reaction Centers. *Proc. Natl. Acad. Sci. USA.* **1998**, *95*, 12306−12311.

(6) Reddy, N. R.; Kolaczkowski, S. V.; Small, G. J. A Photoinduced Persistent Structural Transformation of the Special Pair of a Bacterial Reaction Center. *Science* **1993**, *260*, 68−71.

(7) Cherepy, N. J.; Shreve, A. P.; Moore, L. J.; Franzen, S.; Boxer, S. G.; Mathies, R. a. Near-Infrared Resonance Raman Spectroscopy of the Special Pair and the Accessory Bacteriochlorophylls in Photosynthetic Reaction Centers. *J. Phys. Chem.* **1994**, *98*, 6023−6029.

(8) Yakovlev, A. G.; Shkuropatov, A. Y.; Shuvalov, V. A. Nuclear Wave Packet Motion between P* and P$^+$B$_A^-$ Potential Surfaces with a Subsequent Electron Transfer to H$_A$ in Bacterial Reaction Centers at 90 K. Electron Transfer Pathway. *Biochemistry* **2002**, *41*, 14019−14027.

(9) Shuvalov, V.; Yakovlev, A. Coupling of Nuclear Wavepacket Motion and Charge Separation in Bacterial Reaction Centers. *FEBS Lett.* **2003**, *540*, 26−34.

(10) Moore, L. J.; Zhou, H.; Boxer, S. G. Excited-State Electronic Asymmetry of the Special Pair in Photosynthetic Reaction Center Mutants: Absorption and Stark Spectroscopy. *Biochemistry* **1999**, *38*, 11949−11960.

(11) Cohen Stuart, T.; van Grondelle, R. Multipulse Spectroscopy on the Wild-Type and YM210W Bacterial Reaction Centre Uncovers a New Intermediate State in the Special Pair Excited State. *Chem. Phys. Lett.* **2009**, *474*, 352−356.

(12) Holzapfel, W.; Finkele, U.; Kaiser, W.; Oesterhelt, D.; Scheer, H.; Stilz, H. U.; Zinth, W. Initial Electron-Transfer in the Reaction Center from Rhodobacter Sphaeroides. *Proc. Natl. Acad. Sci. U.S.A.* **1990**, *87*, 5168−5172.

(13) Eisenmayer, T. J.; de Groot, H. J. M.; van de Wetering, E.; Neugebauer, J.; Buda, F. Mechanism and Reaction Coordinate of Directional Charge Separation in Bacterial Reaction Centers. *J. Phys. Chem. Lett* **2012**, *3*, 694−697.

(14) Potter, J. A.; Fyfe, P. K.; Frolov, D.; Wakeham, M. C.; Grondelle, R. V.; Robert, B.; Jones, M. R. Strong Effects of an Individual Water Molecule on the Rate of Light-driven Charge Separation in the Rhodobacter sphaeroides Reaction Center. *Biochemistry* **2005**, *280*, 27155−27164.

(15) Yakovlev, A. G.; Shuvalov, V. A. Electron Transfer in Deuterated Reaction Centers of Rhodobacter Sphaeroides at 90 K According to Femtosecond Spectroscopy Data. *Biochemistry* **2003**, *68*, 603−610.

(16) Daviso, E.; Prakash, S.; Alia, A.; Gast, P.; Neugebauer, J.; Jeschke, G.; Matysik, J. The Electronic Structure of the Primary Electron Donor of Reaction Centers of Purple Bacteria at Atomic Resolution as Observed by Photo-CIDNP ^{13}C NMR. *Proc. Natl. Acad. Sci. U.S.A.* **2009**, *106*, 22281−22286.

(17) Wawrzyniak, P. K.; Beerepoot, M. T. P.; de Groot, H. J. M.; Buda, F. Acetyl Group Orientation Modulates the Electronic Ground-State Asymmetry of the Special Pair in Purple Bacterial Reaction Centers. *Phys. Chem. Chem. Phys.* **2011**, *13*, 10270−10279.

(18) Rautter, J.; Lendzian, F.; Schulz, C.; Fetsch, A.; Kuhn, M.; Lin, X.; Lubitz, W. ENDOR Studies of the Primary Donor Cation Radical in Mutant Reaction Centers of Rhodobacter Sphaeroides with Altered Hydrogen-Bond Interactions. *Biochemistry* **1995**, *34*, 8130−8143.

(19) Car, R.; Parrinello, M. Unified Approach for Molecular Dynamics and Density-Functional Theory. *Phys. Rev. Lett.* **1985**, *55*, 2471.

(20) Marx, D.; Hütter, J. *Ab Initio Molecular Dynamics: Basic Theory and Advanced Methods*; Cambridge University Press: Cambridge, U.K., 2009.

(21) Wu, Q.; Van Voorhis, T. Constrained Density Functional Theory and its Application in Long-Range Electron Transfer. *J. Chem. Theory Comput.* **2006**, *2*, 765−774.

(22) Camara-Artigas; Brune, D.; Allen, J. P. Interactions between Lipids and Bacterial Reaction Centers Determined by Protein Crystallography. *Proc. Natl. Acad. Sci. U.S.A.* **2002**, *99*, 11055−11060.

(23) *CPMD v3.11.1*, Copyright IBM Corp, 1990−2008; Copyright MPI für Festkörperforschung Stuttgart, 1997−2001. http://www.cpmd.org/.

(24) Becke, A. D. Density-Functional Exchange-Energy Approximation with Correct Asymptotic Behavior. *Phys. Rev. A* **1988**, *38*, 3096.

(25) Lee, C.; Yang, W.; Parr, R. G. Development of the Colle-Salvetti Correlation-energy Formula into a Functional of the Electron Density. *Phys. Rev. B* **1988**, *37*, 785.

(26) von Lilienfeld, O. A.; Tavernelli, I.; Rothlisberger, U.; Sebastiani, D. Optimization of Effective Atom Centered Potentials for London Dispersion Forces in Density Functional Theory. *Phys. Rev. Lett.* **2004**, *93*, 153004.

(27) von Lilienfeld, O. A.; Tavernelli, I.; Rothlisberger, U.; Sebastiani, D. Performance of Optimized Atom-centered Potentials for Weakly Bonded Systems Using Density Functional Theory. *Phys. Rev. B* **2005**, *71*, 195119.

(28) Wu, Q.; Van Voorhis, T. Direct Optimization Method to Study Constrained Systems Within Density-functional Theory. *Phys. Rev. A* **2005**, *72*, 024502.

(29) Hirshfeld, F. L. Bonded-atom Fragments for Describing Molecular Charge Densities. *Theor. Chem. Acc.* **1977**, *44*, 129.

(30) Oberhofer, H.; Blumberger, J. Electronic Coupling Matrix Elements From Charge Constrained Density Functional Theory Calculations Using a Plane Wave Basis Set. *J. Chem. Phys.* **2010**, *133*, 244105.

(31) Shuvalov, V. A.; Yakovlev, A. G. Energy Level of P+B- with respect to P* Found from Recombination Fluorescence Measurements in Pheophytin-modified Reaction Centres. *Membr. Cell Biol.* **1998**, *12*, 563−569.

(32) Marcus, A.; Sutin, N. Electron Transfers in Chemistry and Biology. *Biochim. Biophys. Acta* **1985**, *811*, 265.

(33) Moser, C. C.; Keske, J. M.; Warncke, K.; Farid, R. S.; Dutton, L. P. Nature of Biological Electron Transfer. *Nature* **1992**, *355*, 796−802.

(34) Blumberger, J. Free Energies for Biological Electron Transfer from QM/MM Calculation: Method, Application and Critical Assessment. *Phys. Chem. Chem. Phys.* **2008**, *10*, 5651−5667.

(35) Smith, D. M. A.; Rosso, K. M.; Dupuis, M.; Valiev, M.; Straatsma, T. P. Electronic Coupling between Heme Electron-Transfer Centers and Its Decay with Distance Depends Strongly on Relative Orientation. *J. Phys. Chem. B* **2006**, *110*, 15582−15588.

(36) Ivashin, N.; Larsson, S. Trapped Water Molecule in the Charge Separation of a Bacterial Reaction Center. *J. Phys. Chem. B* **2008**, *112*, 12124.

(37) Lendzian, F.; Huber, M.; Isaacson, R. A.; Endeward, B.; Plato, M.; Bönigk, B.; Möbius, K.; Lubitz, W.; Feher, G. The Electronic Structure of the Primary Donor Cation Radical in Rhodobacter Sphaeroides R-26: ENDOR and TRIPLE Resonance Studies in Single Crystals of Reaction Centers. *Biochim. Biophys. Acta* **1993**, *1183*, 139−160.

(38) Deshmukh, S. S.; Akhavein, H.; Williams, J. C.; Allen, J. P.; Kálmán, L. Light-Induced Conformational Changes in Photosynthetic Reaction Centers: Impact of Detergents and Lipids on the Electronic Structure of the Primary Electron Donor. *Biochemistry* **2011**, *50*, 5249−5262.

G

dx.doi.org/10.1021/jp401195t | *J. Phys. Chem. B* XXXX, XXX, XXX−XXX